Rapid Communications | Editors' Suggestion

Uncovering electron-phonon scattering and phonon dynamics in type-I Weyl semimetals

Jennifer Coulter,[1] Gavin B. Osterhoudt,[2] Christina A. C. Garcia,[1] Yiping Wang,[2] Vincent M. Plisson,[2] Bing Shen,[3] Ni Ni,[3] Kenneth S. Burch,[2] and Prineha Narang[1,*]

[1]*John A. Paulson School of Engineering and Applied Sciences, Harvard University, Cambridge, Massachusetts 02138, USA*

[2]*Department of Physics, Boston College, Chestnut Hill, Massachusetts 02467, USA*

[3]*Department of Physics and Astronomy and California NanoSystems Institute, University of California, Los Angeles, California 90095, USA*

(Received 1 July 2019; published 24 December 2019)

Studies of topological semimetals have revealed spectacular transport phenomena spanning extreme magnetoresistance effects and ultrahigh mobilities. As phonon dynamics and electron-phonon scattering play a critical role in the electrical and thermal transport, we pursue a fundamental understanding of these effects in type-I Weyl semimetals NbAs and TaAs. In the temperature-dependent Raman spectra of NbAs we reveal a previously unreported Fano line shape, a signature stemming from the electron-phonon interaction. Additionally, the temperature dependence of the A_1 phonon linewidths in both NbAs and TaAs strongly deviate from the standard model of anharmonic decay. To capture the mechanisms responsible for the observed Fano asymmetry and the atypical phonon linewidth, we present first-principles calculations of the phonon self-energy correction due to the electron-phonon interaction. Through this study of the phonon dynamics and electron-phonon interaction in these Weyl semimetals, we consider specific microscopic pathways which could contribute to the nature of their macroscopic transport.

DOI: 10.1103/PhysRevB.100.220301

Transition-metal monopnictides (TaAs, NbAs, TaP, and NbP) were recently predicted to be Weyl semimetals [1–4] and experimentally confirmed as such via angle-resolved photoemission spectroscopy and quantum oscillation measurements of the characteristic bulk dispersion and surface Fermi arcs [2,5–16]. From this discovery sprang reports of the linear and nonlinear optical response of these materials [17–23] as well as many magnetotransport studies seeking definitive signatures of the chiral anomaly [24–27] in this family [28–36]. While the observation of the chiral anomaly is still a subject of active debate [2,37,38], reports of these materials' giant magnetoresistance and ultrahigh mobilities make understanding their transport behavior and its connections to topological physics a subject of fundamental importance [14–16,28,30–36,39–41].

Yet, despite their critical contributions to electrical transport, the phonon and electron-phonon properties of these materials remain largely unexplored. Therefore, an understanding of transport in these Weyl semimetals demands a thorough investigation of these effects. In this Rapid Communication we present a study of the phonon dynamics in the Weyl semimetals NbAs and TaAs through *ab initio* descriptions and experimental temperature-dependent Raman spectroscopy. These experiments probe the zone-center phonon dynamics and reveal a set of previously unreported Fano line shapes in the B_1 modes of NbAs as well as anomalous temperature dependence of the A_1 mode linewidths in both NbAs and TaAs. For NbAs, we unexpectedly find that both the magnitude of the linewidth and its dependence on temperature are significantly different depending on the surface upon which the Raman measurements are performed. To characterize the mechanisms responsible for the observed Fano line shapes and A_1 linewidths, we present calculations of the electron-phonon coupling in both materials. In particular, we predict the correction to the phonon self-energy as a result of the electron-phonon interaction to better understand how specific phonon modes couple to electronic states in these materials. Stronger electron-phonon coupling is observed in NbAs than in TaAs, which is experimentally consistent with TaAs absence of a Fano line shape and smaller phonon linewidth.

The Raman intensity at 5 K in NbAs and at 10 K in TaAs, collected from *ab* surfaces, are shown in Figs. 1(b) and 1(e), with the full temperature dependence up to 300 K in Figs. 1(a) and 1(d), respectively. The three phonon modes observable on this surface have been identified by their polarization dependence [42] with symmetries $B_1(1)$, $B_1(2)$, and A_1 (in order of increasing energy in NbAs), with the order in TaAs switched to be $B_1(1)$, A_1, and $B_1(2)$ [43]. All three modes are observable across the full temperature range investigated and show no evidence of any structural changes, in agreement with previous studies of the (Nb, Ta)(P, As) family [44]. Noticeable in the two B_1 modes of NbAs is the asymmetry present in each of their line shapes (for details of the fitting see the Supplemental Material [45], as well as Ref. [46]). The asymmetry in each mode is present across the entire temperature range, and notably, the two modes have excess spectral weight on opposite sides, with the lower energy $B_1(1)$ mode having more spectral weight on its low-energy side and the higher energy $B_1(2)$ mode having more spectral weight on the high-energy side, seen in Fig. 1(b).

A Fano line shape is commonly interpreted as a result of the quantum mechanical interference between a discrete excitation and a continuum of states [47,48]. A previous

*prineha@seas.harvard.edu

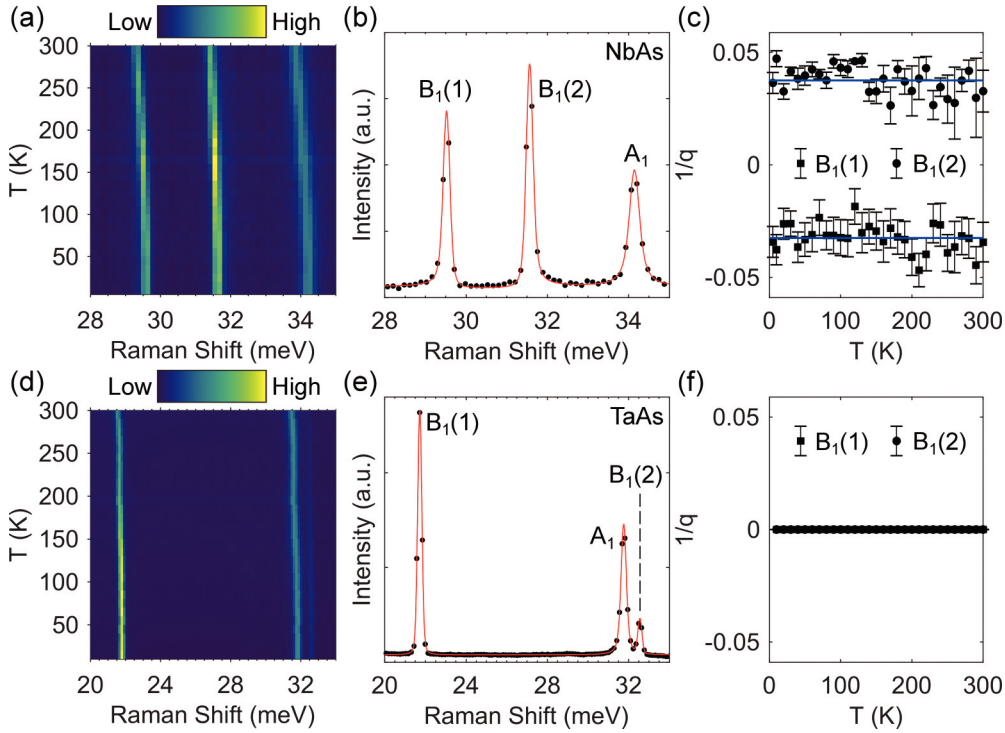

FIG. 1. (a),(d) Temperature and energy dependence of the Raman intensity for NbAs and TaAs, respectively. (b) Raman spectra of NbAs at 5 K in XX polarization. The B_1 phonon modes display a subtle and previously unreported Fano line shape, as quantified by the asymmetry parameter $1/q$ in (c). (e) Raman spectra of TaAs at 10 K in XX polarization, for which no Fano asymmetry is observed. (f) The $1/q$ asymmetry parameter is zero for both B_1 modes in TaAs. Red lines are fits to the experimental data.

investigation of the infrared reflectance of TaAs observed a Fano line shape in the A_1 phonon mode which was interpreted as arising from coupling to the low-energy Weyl fermionlike excitations [48]. The asymmetry in the previously reported TaAs measurements was strongly temperature dependent, while in contrast, the asymmetry observed here in NbAs appears to be nearly temperature independent. In Fig. 1(c) we see that the Fano asymmetry parameter $1/q$ for each mode is nearly independent of temperature, and interestingly, the two modes appear to have nearly the same $1/q$ but of opposite sign with the lower energy $B_1(1)$ mode having $1/q_{\text{avg}} = -0.031 \pm 0.006$ and the higher energy $B_1(2)$ mode having $1/q_{\text{avg}} = 0.037 \pm 0.006$. In comparison, neither of the B_1 modes in TaAs appear to display any Fano asymmetry, nor does the A_1 mode [43] in which it was previously observed in IR measurements [48]. Explicit attempts to fit the TaAs B_1 modes with Fano line shapes result in $1/q$ values that are computationally zero as shown in Fig. 1(f), which confirms the apparent visual symmetry.

While the A_1 modes in NbAs and TaAs appear to lack any asymmetry in their line shapes, their linewidths display atypical temperature-dependent behavior. As shown in Figs. 2(a) and 2(b), we observe that for XX polarization, the A_1 linewidths undergo a sharp increase at temperatures below $\approx$150 K, followed by a decreasing trend towards room temperature in the case of NbAs, while in TaAs this trend appears to reverse and the width starts to increase once more around $\approx$250 K. The standard anharmonic model which describes the decay of optical phonons into two or more acoustic phonons [49] is unable to describe the observed behavior of the A_1 linewidths, which instead suggests a decay of the optical phonons into fermionic excitations, where at high temperatures the Pauli exclusion principle can reduce the number of available states and therefore the linewidth. We note, however, that the dependence of all other measured phonons does match the standard anharmonic prediction (see Supplemental Material [45] for further details and Refs. [50–53] therein).

Motivated by these observations, we evaluate the electron-phonon coupling in both NbAs and TaAs, as in previous works [54–60] (see Supplemental Material [45] for computational details and Refs. [3,4,61–68]). We first compare the calculated zero-temperature phonon energies and those determined from our experimental measurements. In Supplemental Material Table 4 [45] we enumerate these values as well as the percent difference between them for both NbAs and TaAs. We then turn to the calculated imaginary part of the self-energy at room temperature, which is plotted along the phonon dispersions in Fig. 3 for NbAs and TaAs to visually portray how the probability of participating in electron-phonon scattering varies among specific phonon states and between the different materials. From this calculation, we notice an increase in the self-energy of the optical modes near the zone center and see that in NbAs the B_1 modes both experience stronger coupling to the electronic system. While the overall imaginary component of the self-energy is moderate (as typical metals such as Pb, Cu, Pd, or Al feature energies of approximately 0.01–0.2 meV), the calculated value is reasonable given the relatively weak Fano asymmetry observed in experiment. Nonetheless, given the reduced electronic density of states compared to conventional metals, this could be considered a

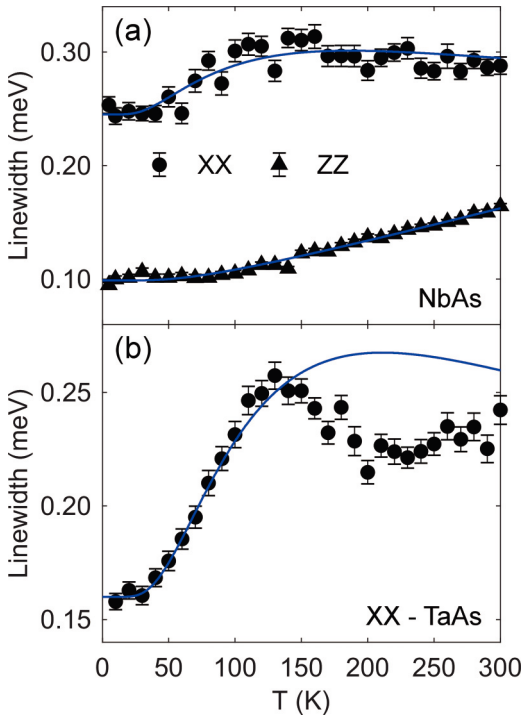

FIG. 2. (a) Temperature dependence of the A_1 phonon mode linewidth in NbAs for XX (ab surface) and ZZ (ac surface) polarization configurations. The ZZ data follows the typical dependence expected from anharmonic decay into acoustic phonons, while the XX data is both noticeably larger and has a distinct temperature dependence. (b) The TaAs A_1 linewidth in XX follows a similar trend to that seen in NbAs. Fits to the XX data are based on a model of phonon decay into electron-hole pairs. While this model captures the dependence over the whole temperature range in NbAs, it only describes the low-temperature behavior of TaAs.

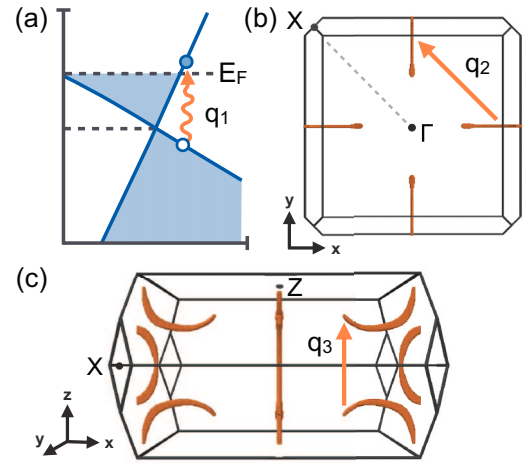

FIG. 4. (a) Shows a possible phonon-mediated transition within a single Weyl cone. (b) and (c) show the Brillouin zone of NbAs, with orange areas indicating the electronic states which are energetically near both another state and E_F (within 38.5 meV, about the largest phonon energy of NbAs). The q denoted on these images indicate possible wave vectors corresponding to those with increased electron-phonon self-energy. Here, q_1 is a wave vector at or near Γ, and q_2 and q_3 are, respectively, along the lines from Γ-X and Γ-Z.

strong electron-phonon effect relative to the number of available electronic states. Similar electron-phonon interaction is predicted in all of the optical modes around 30 meV, despite the asymmetry only arising in the B_1 modes experimentally (for further discussion of the role of symmetry see the Supplemental Material [45]). Comparing these Imℿ calculations for NbAs and TaAs, it is visually apparent that the electron-phonon interaction plays a larger role in the phonons of NbAs than in TaAs. To quantify this, we also present the self-energy specifically at the Γ point for each material and their ratio in Supplemental Material Table 1 [45]. From the ratio of their self-energies we can see that, in general, the effect of the electron-phonon interaction in NbAs is stronger in all phonon modes, consistent with the experimental linewidths and the observation of Fano line shapes in NbAs but not TaAs.

To further understand the role of electron-phonon scattering, we carefully examine the temperature dependence of the A_1 linewidth. As shown in Fig. 2, we find that the nonmonotonic temperature dependence of the A_1 mode linewidth when measured on ab surfaces (XX) of both NbAs and TaAs is well described by a model of phonon decay into electron-hole pairs, as schematically depicted in Fig. 4(a). This is consistent with a previous IR work on TaAs [48], though the previously observed linewidth decreased monotonically with temperature. However, as detailed in the Supplemental Material [45],

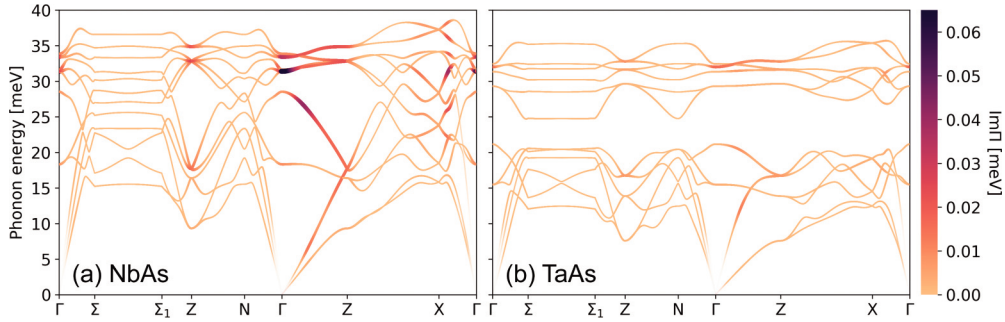

FIG. 3. The correction to the imaginary part of the phonon self-energy due to the electron-phonon interaction at room temperature projected onto the phonon dispersions of (a) NbAs and (b) TaAs. For both materials, there is a notable increase in self-energy at the Γ point, Z point, and along the Γ-X line, offering insight into which phonon modes and wave vectors play a significant role in macroscopic transport. Though the overall calculated self-energy is less for TaAs than NbAs, similar wave vectors show enhanced phonon self-energy in both materials.

we found that by generalizing the model, which was originally developed for the linear Dirac-like system graphene [69], to account for a finite chemical potential and the tilt of the Weyl nodes we were able to capture the features present in our measured temperature dependence. Fits to our data using the generalized model are plotted as blue lines in Figs. 2(a) and 2(b). Overall, this model accounts well for the temperature dependence over the entire investigated temperature range in NbAs, with clear deviations seen at higher temperatures for TaAs. We also note that the larger linewidth in NbAs suggests stronger electron-phonon scattering, consistent with our *ab initio* calculations (Fig. 3). This is further evidenced as the temperature dependence of the A_1 mode energies in NbAs and TaAs indicate similar levels of anharmonicity. The deviations of the data from the model in TaAs likely result from contributions of the W1 node, as it is only $\approx$14 meV [5] below the W2 node, whereas it is considerably lower ($\approx$38 meV [9]) in NbAs.

Interestingly, we find that the unusual linewidth dependence of the NbAs A_1 mode is not observed when the mode is measured with light incident on an *ac* surface. The black triangles in Fig. 2(a), corresponding to the A_1 linewidth as measured in *ZZ*, reveal a monotonically rising temperature dependence—a result that is consistent with anharmonic decay into acoustic phonons [49]. This varying behavior suggests that, unlike the usual approximation that Raman-scattered phonons have zero momentum, the A_1 phonons measured on these two surfaces have different momentum and further that they possess distinct decay channels. One possible explanation is that the phonon decay causes an intraband transition along the linear Weyl bands, and that the anisotropy of the bands along different momentum directions permits energy and momentum conservation to be satisfied for some direction, but not another. While spin conservation would be guaranteed for such transitions, our calculations (detailed in the Supplemental Material [45], using Ref. [70]) find that energy and momentum conservation are not satisfied. This confirms our previous assumption that the electron-hole decay observed in the linewidth dependence must result from interband transitions. This raises an important, as yet unaddressed issue of phonon-induced interband transitions in Weyl semimetals. Namely, since phonons carry zero spin, they should be unable to produce a transition between the two bands with opposite spin which comprise a Weyl node. However, as suggested by recent theoretical work [71], due to crystal anisotropy and their close proximity, the spin polarization of the Weyl nodes in NbAs may not exactly adhere to the predictions for an isolated, ideal Weyl node. In such a scenario, the relaxed spin polarization along one direction may permit optical phonon-induced interband transitions to occur for phonons with, e.g., nonzero q_c, as in our *XX* measurements on an *ab* surface, while preventing similar transitions from occurring for nonzero q_b phonons, as in our *ZZ* measurements on an *ac* surface. While this does provide a self-consistent explanation for the behavior of our observed A_1 linewidths, the present lack of experimental spin-resolved measurements on NbAs leaves confirmation of this mechanism to future investigations.

Having established phonon decay into electron-hole pairs as a significant scattering mechanism in the A_1 modes, we aim to understand the specific scattering pathways which contribute to electron-phonon scattering. As in Figs. 4(b) and 4(c), we select for electronic states which are energetically within a phonon energy of both another state and E_F to visualize the electronic states available for electron-hole generation by a phonon in these materials. We find that the selected states displayed in Fig. 4 correspond well to the wave vectors which display enhanced self-energy along the phonon dispersion. In Fig. 4(a), we show transitions due to $\vec{q}_1$, which represents a wave vector on or very near to Γ, corresponding to the momentum of our optically excited phonons and potentially connecting states within the same Weyl cone or across very closely neighboring pairs. In Fig. 4(b), we show a possible $\vec{q}_2$, connecting k-space locations diagonally across the zone within the same k_z plane via a wave vector along the Γ-X line. In Fig. 4(c), we indicate $\vec{q}_3$, representing transitions in the k_z direction along the Γ-Z line nearly equal to the distance from Γ to Z. These wave vectors fit well with those of strong scattering seen in the self-energy calculation, and in particular, for wave vectors near the Γ-Z line and Γ point, correspond to the k-space distances which connect areas surrounding Weyl cones. While examining the phase space available for phonon decay into electron-hole pairs is not the only consideration necessary for establishing a strong theory of the exact decay mechanism, these results do suggest the existence of inter- and intra-Weyl node-scattering pathways accessible via phonons. Identifying such pathways may enable efforts to observe the chiral anomaly, since internode scattering is required for the system to reach equilibrium [24]. Additionally, similar plots for TaAs show considerably fewer available states, likely related to the weaker electron-phonon effects observed in TaAs (see Supplemental Material Fig. 17 [45]).

Overall, our combined theoretical and experimental study identifies important features of the phonon and electron-phonon properties of these type-I Weyl semimetals. From first-principles calculations of the electron-phonon coupling, we predict the imaginary part of the phonon self-energy due to the electron-phonon interaction and explore specific channels for scattering in NbAs and TaAs. A detailed experimental study of temperature-dependent Raman spectra of NbAs reveals a Fano line shape in the two B_1 zone-center phonon modes and a temperature dependence of the A_1 linewidths in both NbAs and TaAs which deviates strongly from traditional anharmonic phonon models. These complementary predictions and experimental measurements evaluate the role of the electron-phonon interaction and investigate the microscopic scattering processes underlying transport in these type-I Weyl materials.

Calculations and other theory work done by J.C., C.A.C.G, and P.N. was supported by the DOE "Photonics at Thermodynamic Limits" Energy Frontier Research Center under Grant No. DE-SC0019140. Analysis and measurements performed by G.B.O. and work done by K.S.B. was supported by the U.S. Department of Energy (DOE), Office of Science, Office of Basic Energy Sciences under Award No. DE-SC0018675. Raman experiments by Y.W. and V.M.P. were supported by the National Science Foundation through Grant No. DMR-1709987. This research used resources of the National En-

ergy Research Scientific Computing Center, a DOE Office of Science User Facility supported by the Office of Science of the U.S. Department of Energy under Contract No. DE-AC02-05CH11231, as well as resources at the Research Computing Group at Harvard University. J.C. recognizes the support of the DOE Computational Science Graduate Fellowship (CSGF) under Grant No. DE-FG02-97ER25308. C.A.C.G. is supported by the NSF Graduate Research Fellowship Program. Work at UCLA was supported by the U.S. Department of Energy (DOE), Office of Science, Office of Basic Energy Sciences under Award No. DE-SC0011978.

J.C. and G.B.O. contributed equally to this work.

[1] H. Weyl, Z. Phys. **56**, 330 (1929).
[2] N. P. Armitage, E. J. Mele, and A. Vishwanath, Rev. Mod. Phys. **90**, 015001 (2018).
[3] H. Weng, C. Fang, Z. Fang, B. A. Bernevig, and X. Dai, Phys. Rev. X **5**, 011029 (2015).
[4] S.-M. Huang, S.-Y. Xu, I. Belopolski, C.-C. Lee, G. Chang, B. Wang, N. Alidoust, G. Bian, M. Neupane, C. Zhang, S. Jia, A. Bansil, H. Lin, and M. Z. Hasan, Nat. Commun. **6**, 7373 (2015).
[5] S.-Y. Xu, I. Belopolski, N. Alidoust, M. Neupane, G. Bian, C. Zhang, R. Sankar, G. Chang, Z. Yuan, C.-C. Lee, S.-M. Huang, H. Zheng, J. Ma, D. S. Sanchez, B. Wang, A. Bansil, F. Chou, P. P. Shibayev, H. Lin, S. Jia, and M. Z. Hasan, Science **349**, 613 (2015).
[6] B. Q. Lv, H. M. Weng, B. B. Fu, X. P. Wang, H. Miao, J. Ma, P. Richard, X. C. Huang, L. X. Zhao, G. F. Chen, Z. Fang, X. Dai, T. Qian, and H. Ding, Phys. Rev. X **5**, 031013 (2015).
[7] B. Q. Lv, N. Xu, H. M. Weng, J. Z. Ma, P. Richard, X. C. Huang, L. X. Zhao, G. F. Chen, C. E. Matt, F. Bisti, V. N. Strocov, J. Mesot, Z. Fang, X. Dai, T. Qian, M. Shi, and H. Ding, Nat. Phys. **11**, 724 (2015).
[8] L. X. Yang, Z. K. Liu, Y. Sun, H. Peng, H. F. Yang, T. Zhang, B. Zhou, Y. Zhang, Y. F. Guo, M. Rahn, D. Prabhakaran, Z. Hussain, S.-K. Mo, C. Felser, B. Yan, and Y. L. Chen, Nat. Phys. **11**, 728 (2015).
[9] S.-Y. Xu, N. Alidoust, I. Belopolski, Z. Yuan, G. Bian, T.-R. Chang, H. Zheng, V. N. Strocov, D. S. Sanchez, G. Chang, C. Zhang, D. Mou, Y. Wu, L. Huang, C.-C. Lee, S.-M. Huang, B. Wang, A. Bansil, H.-T. Jeng, T. Neupert, A. Kaminski, H. Lin, S. Jia, and M. Z. Hasan, Nat. Phys. **11**, 748 (2015).
[10] S.-Y. Xu, I. Belopolski, D. S. Sanchez, C. Zhang, G. Chang, C. Guo, G. Bian, Z. Yuan, H. Lu, T.-R. Chang, P. P. Shibayev, M. L. Prokopovych, N. Alidoust, H. Zheng, C.-C. Lee, S.-M. Huang, R. Sankar, F. Chou, C.-H. Hsu, H. T. Jeng, A. Bansil, T. Neupert, V. N. Strocov, H. Lin, S. Jia, and M. Z. Hasan, Sci. Adv. **1**, e1501092 (2015).
[11] D.-F. Xu, Y.-P. Du, Z. Wang, Y.-P. Li, X.-H. Niu, Q. Yao, D. Pavel, Z.-A. Xu, X.-G. Wan, and D.-L. Feng, Chin. Phys. Lett. **32**, 107101 (2015).
[12] N. Xu, H. M. Weng, B. Q. Lv, C. E. Matt, J. Park, F. Bisti, V. N. Strocov, D. Gawryluk, E. Pomjakushina, K. Conder, N. C. Plumb, M. Radovic, G. Autès, O. V. Yazyev, Z. Fang, X. Dai, T. Qian, J. Mesot, H. Ding, and M. Shi, Nat. Commun. **7**, 11006 (2016).
[13] S. Souma, Z. Wang, H. Kotaka, T. Sato, K. Nakayama, Y. Tanaka, H. Kimizuka, T. Takahashi, K. Yamauchi, T. Oguchi, K. Segawa, and Y. Ando, Phys. Rev. B **93**, 161112(R) (2016).
[14] N. J. Ghimire, Y. Luo, M. Neupane, D. J. Williams, E. D. Bauer, and F. Ronning, J. Phys.: Condens. Matter **27**, 152201 (2015).
[15] C.. Zhang, C. Guo, H. Lu, X. Zhang, Z. Yuan, Z. Lin, J. Wang, and S. Jia, Phys. Rev. B **92**, 041203(R) (2015).
[16] C. Shekhar, A. K. Nayak, Y. Sun, M. Schmidt, M. Nicklas, I. Leermakers, U. Zeitler, Y. Skourski, J. Wosnitza, Z. Liu, Y. Chen, W. Schnelle, H. Borrmann, Y. Grin, C. Felser, and B. Yan, Nat. Phys. **11**, 645 (2015).
[17] B. Xu, Y. M. Dai, L. X. Zhao, K. Wang, R. Yang, W. Zhang, J. Y. Liu, H. Xiao, G. F. Chen, A. J. Taylor, D. A. Yarotski, R. P. Prasankumar, and X. G. Qiu, Phys. Rev. B **93**, 121110(R) (2016).
[18] L. Wu, S. Patankar, T. Morimoto, N. L. Nair, E. Thewalt, A. Little, J. G. Analytis, J. E. Moore, and J. Orenstein, Nat. Phys. **13**, 350 (2017).
[19] S.-I. Kimura, H. Yokoyama, H. Watanabe, J. Sichelschmidt, V. Süß, M. Schmidt, and C. Felser, Phys. Rev. B **96**, 075119 (2017).
[20] K. Sun, S.-S. Sun, L.-L. Wei, C. Guo, H.-F. Tian, G.-F. Chen, H.-X. Yang, and J.-Q. Li, Chin. Phys. Lett. **34**, 117203 (2017).
[21] D. Neubauer, A. Yaresko, W. Li, A. Löhle, R. Hübner, M. B. Schilling, C. Shekhar, C. Felser, M. Dressel, and A. V. Pronin, Phys. Rev. B **98**, 195203 (2018).
[22] S. Patankar, L. Wu, B. Lu, M. Rai, J. D. Tran, T. Morimoto, D. E. Parker, A. G. Grushin, N. L. Nair, J. G. Analytis, J. E. Moore, J. Orenstein, and D. H. Torchinsky, Phys. Rev. B **98**, 165113 (2018).
[23] G. B. Osterhoudt, L. K. Diebel, M. J. Gray, X. Yang, J. Stanco, X. Huang, B. Shen, N. Ni, P. J. W. Moll, Y. Ran, and K. S. Burch, Nat. Mater. **18**, 471 (2019).
[24] H. B. Nielsen and M. Ninomiya, Phys. Lett. B **130**, 389 (1983).
[25] A. A. Zyuzin and A. A. Burkov, Phys. Rev. B **86**, 115133 (2012).
[26] D. T. Son and B. Z. Spivak, Phys. Rev. B **88**, 104412 (2013).
[27] S. A. Parameswaran, T. Grover, D. A. Abanin, D. A. Pesin, and A. Vishwanath, Phys. Rev. X **4**, 031035 (2014).
[28] X. Huang, L. Zhao, Y. Long, P. Wang, D. Chen, Z. Yang, H. Liang, M. Xue, H. Weng, Z. Fang, X. Dai, and G. Chen, Phys. Rev. X **5**, 031023 (2015).
[29] C.-L. Zhang, S.-Y. Xu, I. Belopolski, Z. Yuan, Z. Lin, B. Tong, G. Bian, N. Alidoust, C.-C. Lee, S.-M. Huang, T.-R. Chang, G. Chang, C.-H. Hsu, H.-T. Jeng, M. Neupane, D. S. Sanchez, H. Zheng, J. Wang, H. Lin, C. Zhang, H.-Z. Lu, S.-Q. Shen, T. Neupert, M. Z. Hasan, and S. Jia, Nat. Commun. **7**, 10735 (2015).
[30] J. Hu, J. Y. Liu, D. Graf, S. M. A. Radmanesh, D. J. Adams, A. Chuang, Y. Wang, I. Chiorescu, J. Wei, L. Spinu, and Z. Q. Mao, Sci. Rep. **6**, 18674 (2016).
[31] F. Arnold, C. Shekhar, S.-C. Wu, Y. Sun, R. D. dos Reis, N. Kumar, M. Naumann, M. O. Ajeesh, M. Schmidt, A. G. Grushin, J. H. Bardarson, M. Baenitz, D. Sokolov, H. Borrmann, M. Nicklas, C. Felser, E. Hassinger, and B. Yan, Nat. Commun. **7**, 11615 (2016).

[32] J. Du, H. Wang, Q. Chen, Q. Mao, R. Khan, B. Xu, Y. Zhou, Y. Zhang, J. Yang, B. Chen, C. Feng, and M. Fang, Sci. China: Phys. Mech. Astron. **59**, 657406 (2016).
[33] Z. Wang, Y. Zheng, Z. Shen, Y. Lu, H. Fang, F. Sheng, Y. Zhou, X. Yang, Y. Li, C. Feng, and Z.-A. Xu, Phys. Rev. B **93**, 121112(R) (2016).
[34] A. C. Niemann, J. Gooth, S.-C. Wu, S. Bäßler, P. Sergelius, R. Hühne, B. Rellinghaus, C. Shekhar, V. Süß, M. Schmidt, C. Felser, B. Yan, and K. Nielsch, Sci. Rep. **7**, 43394 (2017).
[35] C.-L. Zhang, Z. Yuan, Q.-D. Jiang, B. Tong, C. Zhang, X. C. Xie, and S. Jia, Phys. Rev. B **95**, 085202 (2017).
[36] Sudesh, P. Kumar, P. Neha, T. Das, and S. Patnaik, Sci. Rep. **7**, 46062 (2017).
[37] R. D. dos Reis, M. O. Ajeesh, N. Kumar, F. Arnold, C. Shekhar, M. Naumann, M. Schmidt, M. Nicklas, and E. Hassinger, New J. Phys. **18**, 085006 (2016).
[38] Y. Li, Z. Wang, P. Li, X. Yang, Z. Shen, F. Sheng, X. Li, Y. Lu, Y. Zheng, and Z.-A. Xu, Front. Phys. **12**, 127205 (2017).
[39] Y. Luo, N. J. Ghimire, M. Wartenbe, H. Choi, M. Neupane, R. D. McDonald, E. D. Bauer, J. Zhu, J. D. Thompson, and F. Ronning, Phys. Rev. B **92**, 205134 (2015).
[40] J. Xiang, S. Hu, Z. Song, M. Lv, J. Zhang, L. Zhao, W. Li, Z. Chen, S. Zhang, J.-T. Wang, Y.-F. Yang, X. Dai, F. Steglich, G. Chen, and P. Sun, Phys. Rev. X **9**, 031036 (2019).
[41] Z. Song and X. Dai, Phys. Rev. X **9**, 021053 (2019).
[42] H. W. Liu, P. Richard, L. X. Zhao, G.-F. Chen, and H. Ding, J. Phys.: Condens. Matter **28**, 295401 (2016).
[43] H. W. Liu, P. Richard, Z. D. Song, L. X. Zhao, Z. Fang, G.-F. Chen, and H. Ding, Phys. Rev. B **92**, 064302 (2015).
[44] Y. Luo, N. J. Ghimire, E. D. Bauer, J. D. Thompson, and F. Ronning, J. Phys.: Condens. Matter **28**, 055502 (2016).
[45] See Supplemental Material at http://link.aps.org/supplemental/10.1103/PhysRevB.100.220301 for more experimental and computational details, as well as a discussion of the intraband transition calculations.
[46] Y. Tian, A. A. Reijnders, G. B. Osterhoudt, I. Valmianski, J. G. Ramirez, C. Urban, R. Zhong, J. Schneeloch, G. Gu, I. Henslee, and K. S. Burch, Rev. Sci. Instrum. **87**, 043105 (2016).
[47] U. Fano, Phys. Rev. **124**, 1866 (1961).
[48] B. Xu, Y. M. Dai, L. X. Zhao, K. Wang, R. Yang, W. Zhang, J. Y. Liu, H. Xiao, G. F. Chen, S. A. Trugman, J.-X. Zhu, A. J. Taylor, D. A. Yarotski, R. P. Prasankumar, and X. G. Qiu, Nat. Commun. **8**, 14933 (2017).
[49] P. G. Klemens, Phys. Rev. **148**, 845 (1966).
[50] M. Chandrasekhar, J. B. Renucci, and M. Cardona, Phys. Rev. B **17**, 1623 (1978).
[51] M. Cardona, F. Cerdeira, and T. A. Fjeldly, Phys. Rev. B **10**, 3433 (1974).
[52] O. Kashuba and V. I. Fal'ko, New J. Phys. **14**, 105016 (2012).
[53] M. Balkanski, R. F. Wallis, and E. Haro, Phys. Rev. B **28**, 1928 (1983).
[54] C. J. Ciccarino, T. Christensen, R. Sundararaman, and P. Narang, Nano Lett. **18**, 5709 (2018).
[55] P. Narang, L. Zhao, S. Claybrook, and R. Sundararaman, Adv. Opt. Mater. **5**, 1600914 (2017).
[56] J. Coulter, R. Sundararaman, and P. Narang, Phys. Rev. B **98**, 115130 (2018).
[57] A. M. Brown, R. Sundararaman, P. Narang, W. A. Goddard, and H. A. Atwater, ACS Nano **10**, 957 (2016).
[58] S. N. Shirodkar, M. Mattheakis, P. Cazeaux, P. Narang, M. Soljačić, and E. Kaxiras, Phys. Rev. B **97**, 195435 (2018).
[59] A. M. Brown, R. Sundararaman, P. Narang, W. A. Goddard, and H. A. Atwater, Phys. Rev. B **94**, 075120 (2016).
[60] R. Sundararaman, P. Narang, A. S. Jermyn, W. A. Goddard III, and H. A. Atwater, Nat. Commun. **5**, 5788 (2014).
[61] F. Giustino, Rev. Mod. Phys. **89**, 015003 (2017).
[62] R. Sundararaman, K. Letchworth-Weaver, K. Schwarz, D. Gunceler, Y. Ozhabes, and T. A. Arias, SoftwareX **6**, 278 (2017).
[63] A. Dal Corso, Comput. Mater. Sci. **95**, 337 (2014).
[64] A. M. Rappe, K. M. Rabe, E. Kaxiras, and J. D. Joannopoulos, Phys. Rev. B **41**, 1227 (1990).
[65] J. P. Perdew, A. Ruzsinszky, G. I. Csonka, O. A. Vydrov, G. E. Scuseria, L. A. Constantin, X. Zhou, and K. Burke, Phys. Rev. Lett. **100**, 136406 (2008).
[66] N. Marzari, D. Vanderbilt, A. De Vita, and M. C. Payne, Phys. Rev. Lett. **82**, 3296 (1999).
[67] F. Giustino, M. L. Cohen, and S. G. Louie, Phys. Rev. B **76**, 165108 (2007).
[68] C.-C. Lee, S.-Y. Xu, S.-M. Huang, D. S. Sanchez, I. Belopolski, G. Chang, G. Bian, N. Alidoust, H. Zheng, M. Neupane, B. Wang, A. Bansil, M. Z. Hasan, and H. Lin, Phys. Rev. B **92**, 235104 (2015).
[69] M. Lazzeri, S. Piscanec, F. Mauri, A. C. Ferrari, and J. Robertson, Phys. Rev. B **73**, 155426 (2006).
[70] C. A. C. Garcia, J. Coulter, and P. Narang, arXiv:1907.04348.
[71] D. Grassano, O. Pulci, E. Cannuccia, and F. Bechstedt, arXiv:1906.12231.